Elastic scattering and particle production in two-prong $\pi^- p$ interactions at 8 GeV/c

T. Kitagaki, S. Tanaka, H. Yuta, K. Abe, K. Hasegawa, A. Yamaguchi, T. Nozaki,[a]
K. Tamai, T. Maruyama,[b] R. Kikuchi,[c] Y. Unno, and Y. Otani
Tohoku University, Sendai 980, Japan

F. Barreiro,[d] O. Benary,[e] J. E. Brau,[f] R. Dolfini,[g] E. S. Hafen,
P. Haridas, D. Hochman,[h] M. F. Hodous,[i] R. I. Hulsizer,
V. Kistiakowsky, A. Napier,[b] S. Noguchi,[j] S. H. Oh, I. A. Pless, J. P. Silverman,[k]
P. C. Trepagnier,[l] J. Wolfson,[m] Y. Wu,[n] and R. K. Yamamoto
Massachusetts Institute of Technology, Cambridge, Massachusetts 02139

H. O. Cohn
Oak Ridge National Laboratory, Oak Ridge, Tennessee 37830

W. M. Bugg, G. T. Condo, T. Handler, and E. L. Hart
University of Tennessee, Knoxville, Tennessee 37916
(Received 11 January 1982)

Results of a high-statistics study of elastic scattering and meson resonances produced by $\pi^- p$ interactions at 8 GeV/c are presented. Large statistics and small systematic errors permit examination of the complete kinematic region. Total differential cross sections are given for $\rho^{0,-}$, f^0, $g^{0,-}$, $\Delta^{\pm}$, Δ^0, and N^* resonances. Spin-density matrix elements and Legendre-polynomial moments are given for ρ, f, and Δ resonances. The results for ρ^0 and f^0 resonances are compared with the predictions of a Regge-pole-exchange model. Properties of the above resonances are compared and discussed. In particular, we present evidence that the ρ^0 and f^0 production mechanisms are similar. The similarity of the g^0 t distribution to that of the ρ^0 and f^0 suggests a common production mechanism for all three resonances.

I. INTRODUCTION

In this paper we report results on a high-statistics study of the reaction

$$\pi^- p \to \pi^- p \ , \tag{1}$$

$$\pi^- p \to \pi^- \pi^0 p \ , \tag{2}$$

$$\pi^- p \to \pi^- \pi^+ n \tag{3}$$

at 8 GeV/c incident π^- momentum. The data used in this experiment were obtained from the measurement of two-prong events in photographs taken in the SLAC 82-in. hydrogen-filled bubble chamber with an incident π^- beam of 8 GeV/c nominal momentum. About 7×10^5 pictures, which correspond to a total of 3×10^5 two-prong events ($\sim$20 events/μb), are involved in this study.

Experimental details and cross sections for reactions (1)–(3) are given in Sec. II. Section III contains the analysis of the elastic-scattering sample. The separation of events from reactions (2) and (3) into various subchannels is given in Sec. IV. Section V deals with the analysis of the resonances produced in reactions (2) and (3). Spin-density-matrix elements and unnormalized Legendre-polynomial moments are presented as a function of t' for ρ, f, and Δ resonances. In addition, the results for ρ^0 and f^0 production are compared with a Regge-exchange model involving Regge-cut contributions along with π and A_2 exchanges.

TABLE I. Cross sections for the reaction $\pi^- p$ at 8 GeV/c leading to two-prong events.

Reaction	Number of events (after cuts)	Cross section (μb)
$\pi^- p \to \pi^- p$	72 340	5070±110
$\pi^- p \to \pi^- \pi^0 p$	12 818	733± 20
$\pi^- p \to \pi^- \pi^+ n$	17 594	992± 26

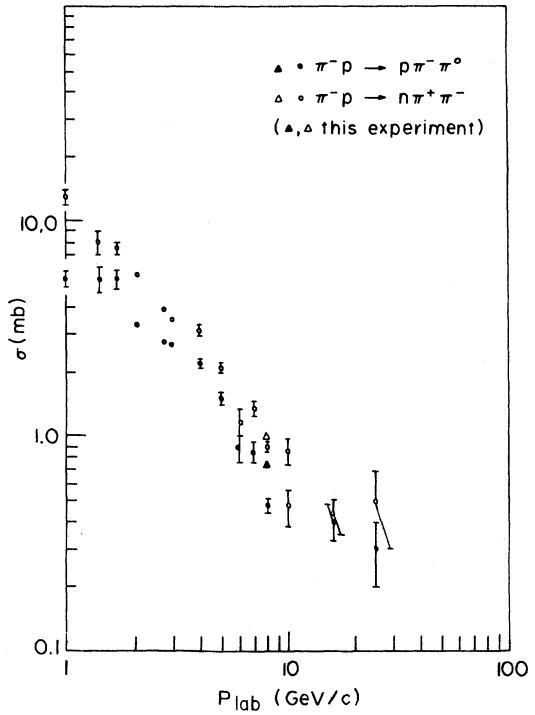

FIG. 1. Cross sections for the reactions $\pi^- p \to \pi^- \pi^0 p$ and $\pi^- p \to n\pi^+\pi^-$ as a function of the incident π^- laboratory momentum.

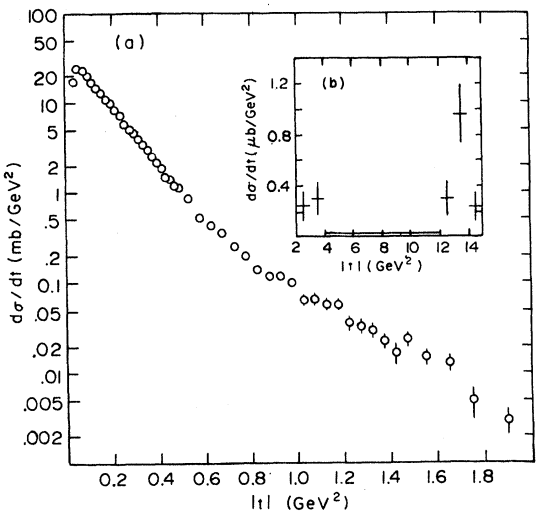

FIG. 2. Differential cross section $d\sigma/dt$ for elastic scattering. (a) Results for $0.0 \leq |t| \leq 2.0$ GeV^2. (b) Results for $2.0 \leq |t| \leq 15.0$ GeV^2.

TABLE II. Elastic-differential-cross-section parameters.

(a)

Incident momentum (GeV/c)	$\|t\|$ range (GeV^2)	A (mb/GeV^2)	B (GeV^{-2})
5[a]	0.15–0.80	44 ±4	7.4 ±0.2
2.3–6[a]	~0.5		7.4 ±0.2
6[b]	0.05–0.44	40.2 ±0.6	7.70 ±0.08
8[b]	0.20–0.35	35.9 ±1.6	7.65 ±0.32
8.5[a]	0.05–0.50	33.8 ±0.74	7.519±0.008
12.4[a]	0.09–0.50	31.03±0.73	7.677±0.09

(b)

Incident momentum (GeV/c)	$\|u\|$ range (GeV^2)	A (μb/GeV^2)	B (GeV^{-2})
5.9[c]	~0.8	4.94±0.12	3.72±0.08
6[c]	~1.0	4.2 ±0.3	2.7 ±0.3
8[b]	~0.35	6.6 ±2.9	3.3 ±2.2
8[c]		3.75±0.35	3.16±0.24
9.9[c]	~0.8	1.70±0.06	4.05±0.08

[a]See Ref. 3.
[b]This experiment.
[c]See Ref. 4.

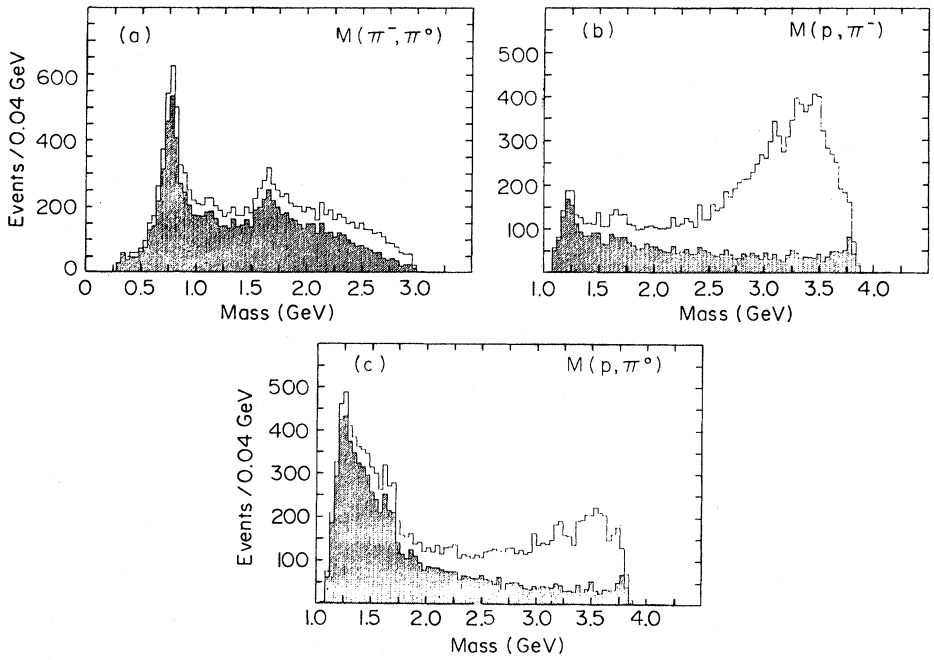

FIG. 3. Two-body effective masses from the reaction $\pi^- p \to \pi^- \pi^0 p$. (a) $M(\pi^-\pi^0)$ with shaded events for $|t'_{p,p}| \leq 0.4$ GeV^2; (b) $M(p\pi^-)$ with shaded events for $|t'_{\pi^-,\pi^0}| \leq 0.4$ GeV^2; (c) $M(p\pi^0)$ with shaded events for $|t'_{\pi^-,\pi^-}| \leq 0.4$ GeV^2.

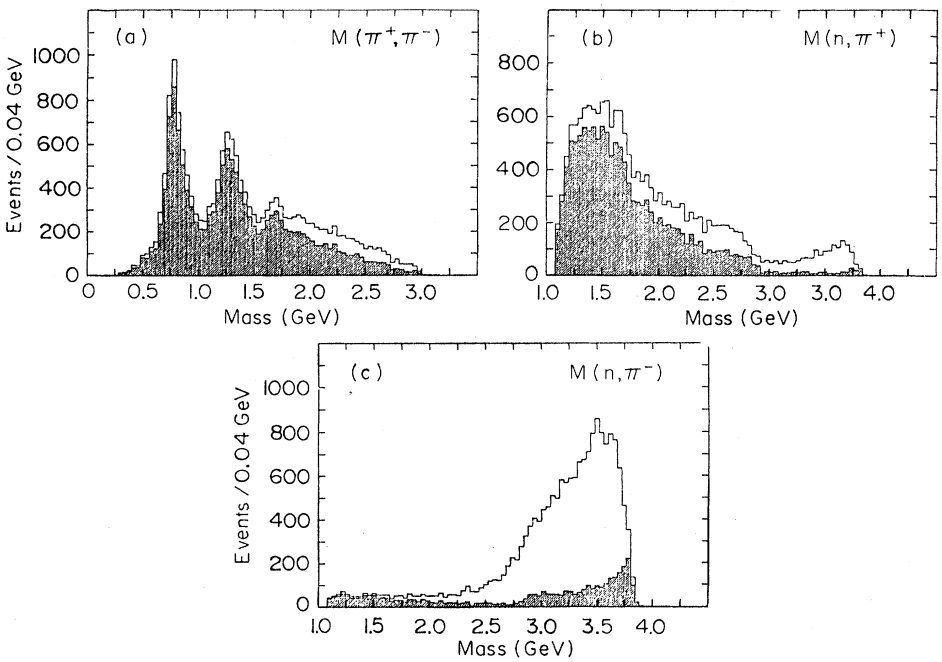

FIG. 4. Two-body effective masses from the reaction $\pi^- p \to \pi^+ \pi^- n$. (a) $M(\pi^+\pi^-)$ with shaded events for $|t'_{p,n}| \leq 0.4$ GeV^2; (b) $M(\pi^+ n)$ with shaded events for $|t'_{\pi^-,\pi^-}| \leq 0.4$ GeV^2; (c) $M(\pi^- n)$ with shaded events for $|t'_{\pi^-,\pi^+}| \leq 0.4$ GeV^2.

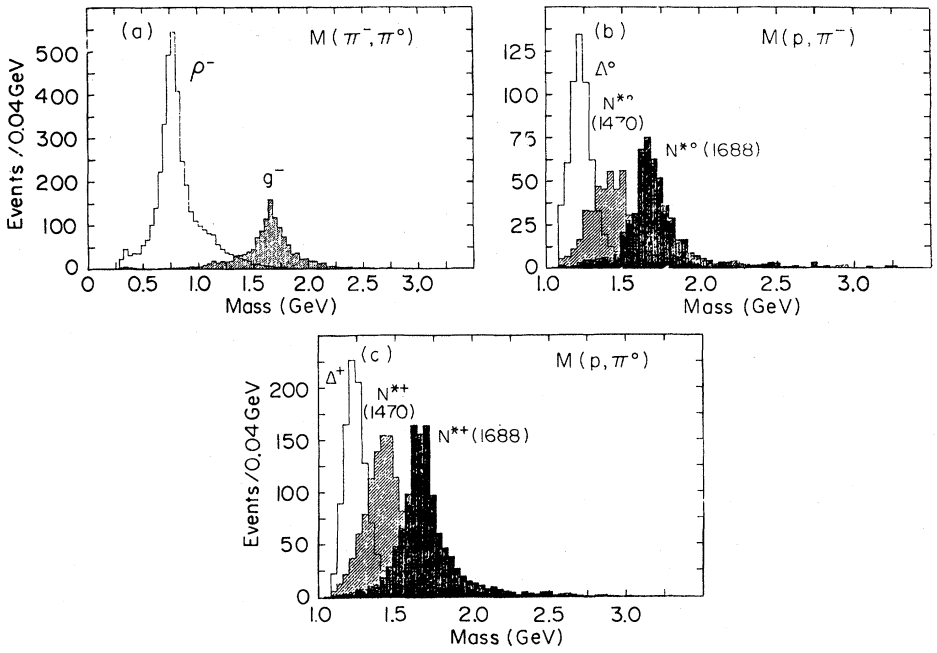

FIG. 5. Two-body effective masses for resonances separated by the prism-plot technique in the reaction $\pi^- p \to \pi^- \pi^0 p$. (a) $M(\pi^-\pi^0)$ for ρ^- and g^- (cross-hatched); (b) $M(p\pi^-)$ for $^-\Delta^0$, $N^{0*}(1470)$ (cross-hatched); $N^{0*}(1688)$ (shaded); (c) $M(p\pi^0)$ for Δ^+,$N^{+*}(1470)$ (cross-hatched), $N^{+*}(1688)$ (shaded).

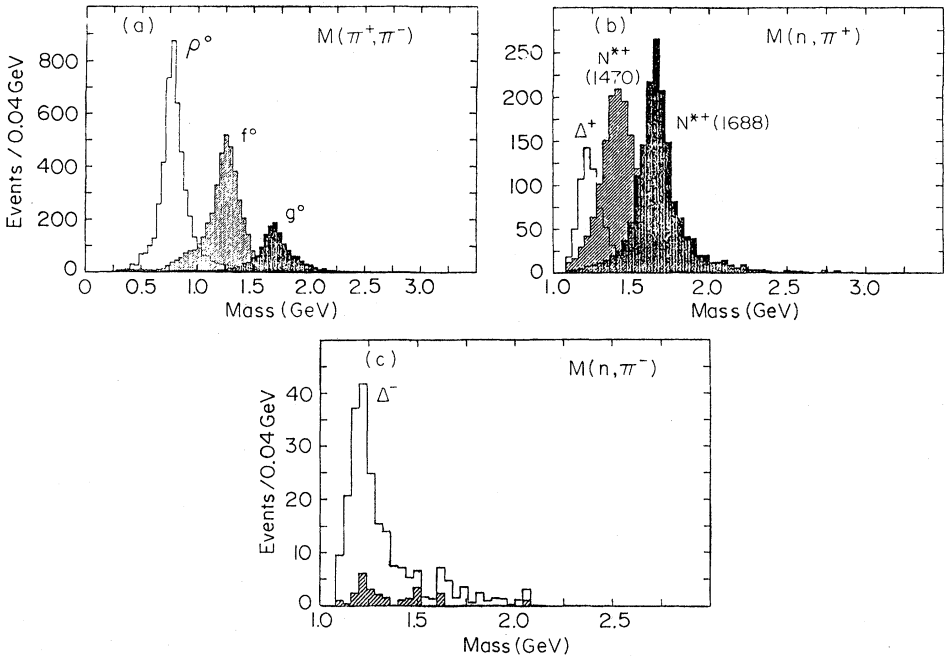

FIG. 6. Two-body effective masses for resonances separated by the prism-plot technique in the reaction $\pi^- p \to \pi^+ \pi^- n$. (a) $M(\pi^+\pi^-)$ for ρ^0, f^0 (cross-hatched), and g^0 (shaded); (b) $M(\pi^+ n)$ for Δ^+, $N^{+*}(1470)$ (cross-hatched), and $N^{+*}(1688)$ (shaded); (c) $M(\pi^- n)$ for Δ^-. Cross-hatched histogram is for $|t'_{\pi^-,\Delta^-}| \leq 0.4$ GeV.

TABLE III. Channel cross sections. DD refers to a nonresonant diffractively produced enhancement.

Reaction	Channel	σ (mb)
$\pi^-p\to p\pi^-\pi^0$	$p\rho^-$	0.222 ±0.008
	pg^-	0.070 ±0.003
	$\Delta^+\pi^-$	0.061 ±0.003
	$\Delta^0\pi^0$	0.036 ±0.005
	$(DD)^+\pi^-$	0.098 ±0.003
	$\pi^0N^{*0}(1688)$	0.028 ±0.003
	$\pi^-N^{*+}(1688)$	0.069 ±0.003
	$\pi^0N^{*0}(1470)$	0.029 ±0.002
	$\pi^-N^{*+}(1470)$	0.069 ±0.002
$\pi^-p\to n\pi^+\pi^-$	$n\rho^0$	0.278 ±0.008
	nf $(f\to\pi^+\pi^-)$	0.245 ±0.007
	ng^0	0.087 ±0.003
	$(DD)^+\pi^-$	0.095 ±0.003
	$\Delta^+\pi^-$	0.038 ±0.002
	$\Delta^-\pi^+$	0.012 ±0.003
	$N^{*+}(1470)\pi^-$	0.092 ±0.003
	$N^{*+}(1688)\pi^-$	0.093 ±0.003
	$\Delta^-\pi^+$(baryon E)	0.0017±0.002

II. EXPERIMENTAL DETAILS

The events were measured by Precision Encoding Pattern Recognition (PEPR) at MIT, by the Spiral Reader at Tennessee, and by Hough-Powell Devices (HPD's) as well as manually at Tohoku.

Hypothesis testing was done by kinematic fits on the following reactions:

$$\pi^-p\to\pi^-p \quad (4C) \tag{1}$$

$$\pi^-p\to\pi^-\pi^0p \quad (1C) \tag{2}$$

$$\pi^-p\to\pi^-\pi^+n \quad (1C) \tag{3}$$

$$\pi^-p\to\pi^-\pi^+\text{MM} \quad (0C) \tag{4}$$

$$\pi^-p\to\pi^-p\text{MM} \quad (0C) \tag{5}$$

(MM stands for missing mass, and 4C, 1C, and 0C for four, one, and zero constraints, respectively.)

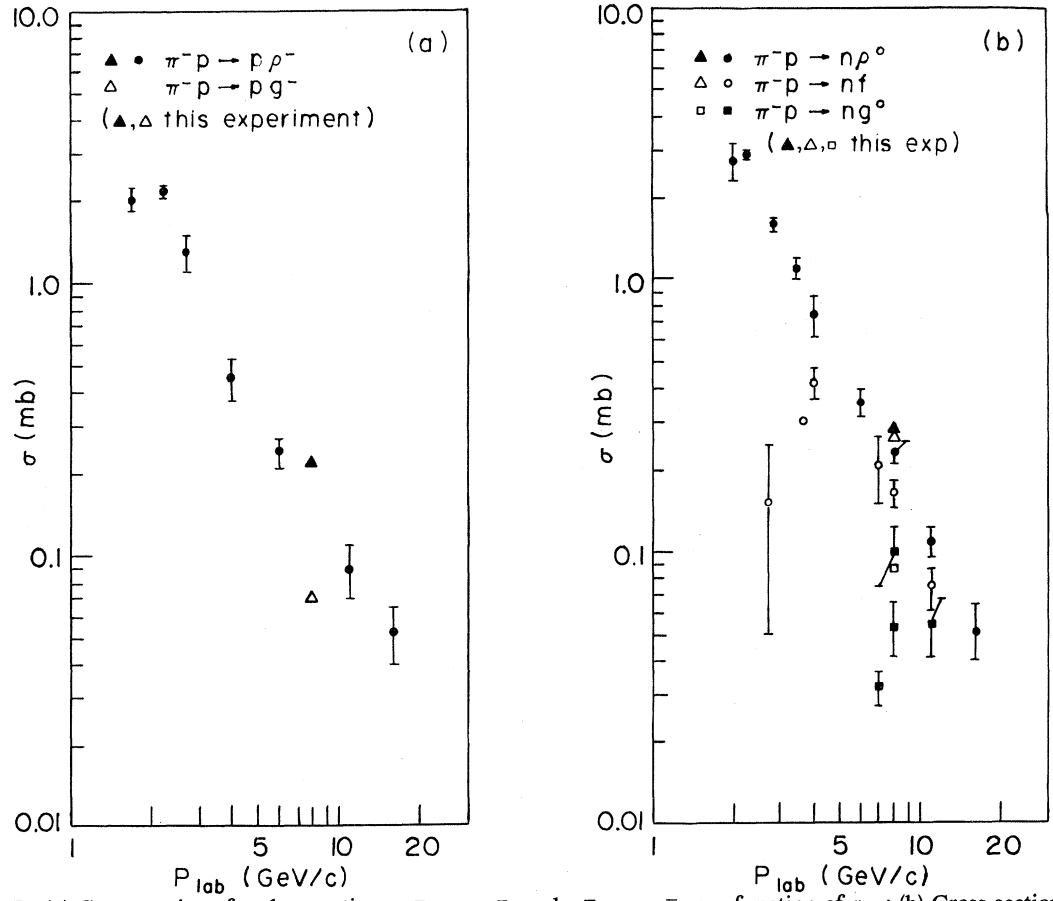

FIG. 7. (a) Cross sections for the reactions $\pi^-p\to p\rho^-$, and $\pi^-p\to pg^-$ as a function of p_{lab}; (b) Cross sections for the reactions $\pi^-p\to\rho^0n$), $\pi^-p\to nf^0$ (corrected for all f^0 decay modes) and $\pi^-p\to g^0n$; (c) Cross sections for the reactions $\pi^-p\to\pi^-\Delta^+\to\pi^-\pi^0p$, $\pi^-p\to\pi^-\Delta^+\to\pi^-\pi^+n$, and $\pi^-p\to\pi^+\Delta^-$.

TABLE IV. Slopes B of t' distributions.

Final state	Resonance	Range (GeV^2)	B (GeV^{-2})	χ^2/DF
$p\pi^-\pi^0$	ρ^-	0.04 −0.38	7.85±0.23	1.63
	g^-	0.0 −0.40	7.41±0.30	0.71
	Δ^+	0.0 −0.40	10.08±0.39	0.84
	Δ^0	0.0 −0.40	7.89±0.43	0.96
	$N^{*+}(1470)$	0.0 −0.40	5.98±0.31	0.57
	$N^{*0}(1470)$	0.0 −0.40	6.38±0.54	1.16
	$N^{*+}(1688)$	0.0 −0.40	2.47±0.29	0.60
	$N^{*0}(1688)$	0.0 −0.40	4.31±0.55	0.63
$n\pi^+\pi^-$	ρ^0	0.0 −0.20	11.88±0.33	2.51
	f	0.0 −0.40	9.94±0.20	1.78
	g^0	0.0 −0.40	8.57±0.31	1.27
	Δ^+	0.0 −0.40	11.59±0.55	0.15
	Δ^-	0.0 −0.40	8.56±0.92	0.37
	$N^{*+}(1470)$	0.0 −0.40	6.12±0.28	0.44
	$N^{*+}(1688)$	0.0 −0.40	1.51±0.25	0.51

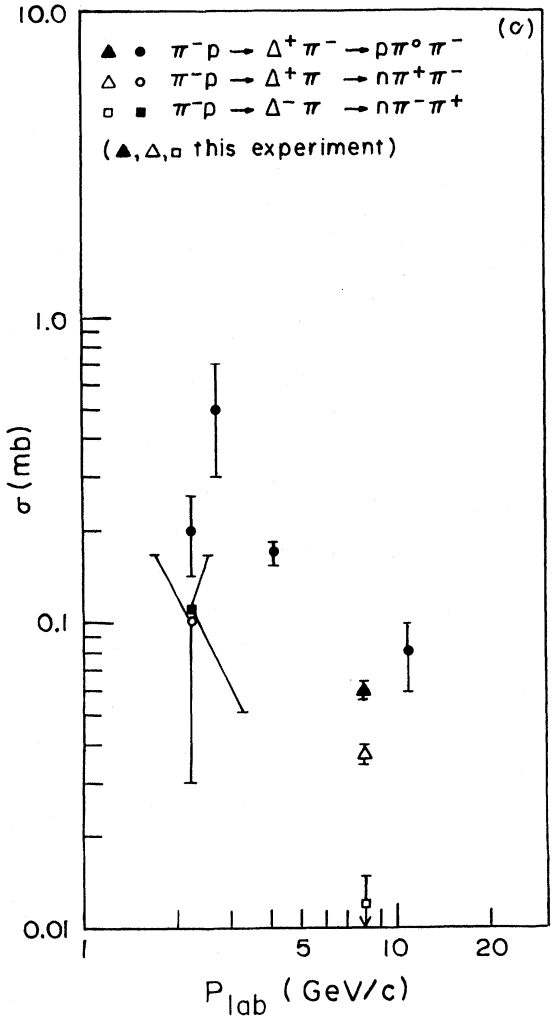

FIG. 7. (*Continued.*)

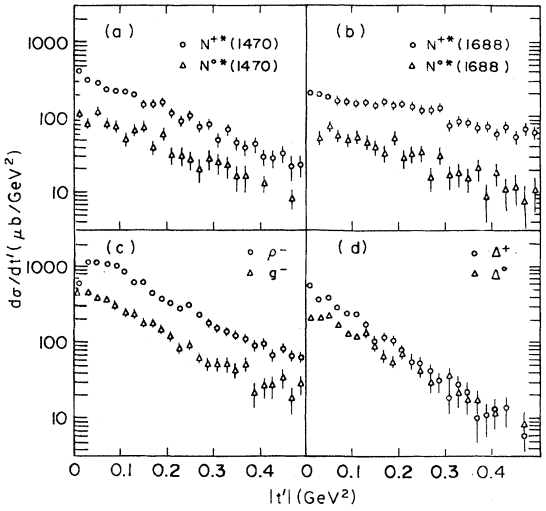

FIG. 8. The distribution $d\sigma/dt'$ in μb/GeV^2 for resonances in the reaction $\pi^- p \to \pi^- \pi^0 p$.

A small fraction of elastic events with high χ^2 contaminates the 1C channels. This contamination has been corrected for, and the corresponding number of events has been apportioned to the elastic channel for cross-section determination.

Events fitting the 1C hypotheses with confidence level $\geq 4\%$ were accepted and the majority of ambiguities between reactions (2) and (3) were resolved by utilizing ionization measurements of the positive track when its momentum was less than 1200 MeV/c, while the remaining ambiguities were resolved on the basis of best χ^2. The contamination to the 1C events due to the 0C events of reactions (4) and (5) was removed by imposing cuts on the square of the missing mass as calculated from the measured charged-particle momenta.

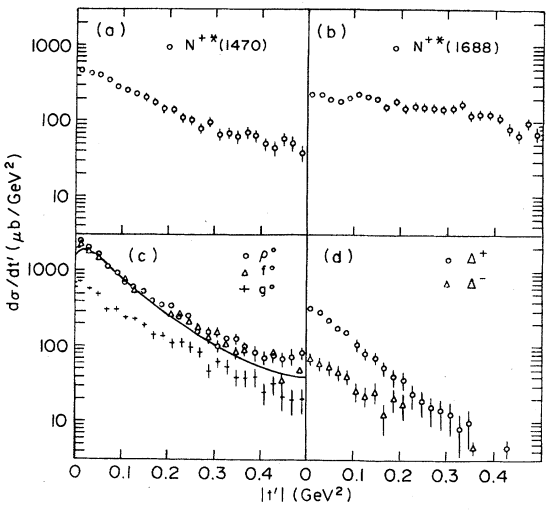

FIG. 9. The distribution $d\sigma/dt'$ in μb/GeV^2 for resonances in the reaction $\pi^- p \to \pi^+ \pi^- n$. Solid curve in (c) represents the prediction of Irving and Michael (Ref. 8) for ρ^0.

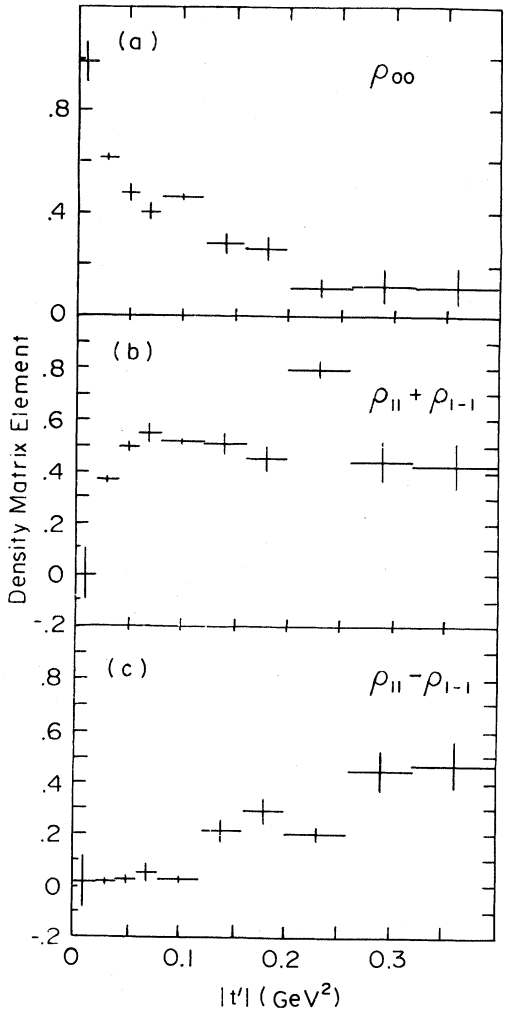

FIG. 10. The ρ^- density-matrix elements in the helicity frame in the reaction $\pi^- p \to \pi^- \pi^0 p$. (a) ρ_{00}; (b) $\rho_{11}+\rho_{1-1}$; (c) $\rho_{11}-\rho_{1-1}$.

Table I displays the number of events found within a restricted fiducial volume and used for the analysis of reactions (1)—(3). Also displayed are the values of the cross sections for these reactions. These cross sections are plotted in Fig. 1 as a function of the incident π^- momentum, and the measurements of this experiment agree with those of the other experiments within their errors.[1] The relative sizes of the statistical errors for this experiment are negligible.

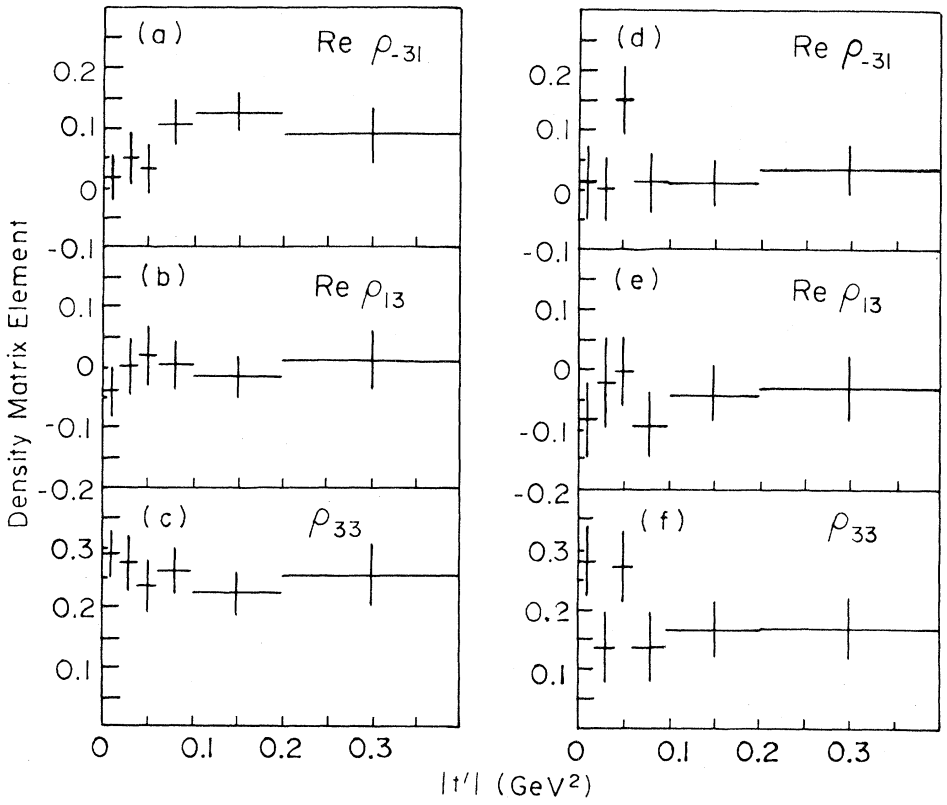

FIG. 11. The Δ^+ and Δ^0 density-matrix elements in the Gottfried-Jackson frame in the reaction $\pi^- p \to \pi^- \pi^0 p$. (a) Re$\rho_{-3,1}$; (b) Re$\rho_{13}$; (c) ρ_{33}; (d) Reρ_{-31}; (e) Reρ_{13}; (f) ρ_{33}. (a)–(c) refer to Δ^+ and (d)–(f) refer to Δ^0.

III. ELASTIC SCATTERING

For the elastic-scattering analysis [reaction (1)], events were selected on the basis of an acceptable χ^2 in the kinematic fitting of the reaction $\pi^- p \to \pi^- p$. About 72 000 events were found which constitute a large enough sample to obtain data points of the differential cross section for the entire t region.

The differential cross section $d\sigma/dt$ is shown in Fig. 2(a) for the forward t region. The data were corrected for events lost due to large dip angles of outgoing tracks. We have made a fit to the function $d\sigma/dt = Ae^{-B|t|}$ in the $|t|$ region between 0.20 and 0.35 GeV^2. The results of the fit constrained to the cross section of Ref. 2 give the optical point with the value $A = 35.9 \pm 1.6$ mb GeV^{-2} and slope parameter $B = 7.65 \pm 0.32$ GeV^{-2}. Table II(a) shows the optical-point and slope parameters for a number of $\pi^- p$ elastic-scattering experiments[3] for incident pion momenta from 4 to 12.4 GeV/c. As can be seen, our parameters agree with those results. In particular, the slope parameter stays fairly constant over this momentum range for our selected t interval, and the optical-point values tend to decrease with increasing incident-beam momentum.

Figure 2(b) shows the differential cross section for the large t. The backward scattering cross section $d\sigma/du = Ae^{-B|u|}$ yields parameters $A = 6.6 \pm 2.9$ mb GeV^{-2} and $B = 3.3 \pm 2.2$ GeV^{-2}. Table II(b) compares our results with those of other experiments[4] near our incident momentum.

In summary, we see the same gross structures seen in other experiments.[3,4]

IV. RESONANCE-PRODUCTION CROSS SECTIONS IN TWO-PRONG INELASTIC CHANNELS [REACTIONS (2) AND (3)]

The two-body effective-mass distributions are shown in Figs. 3 and 4, respectively. The shaded

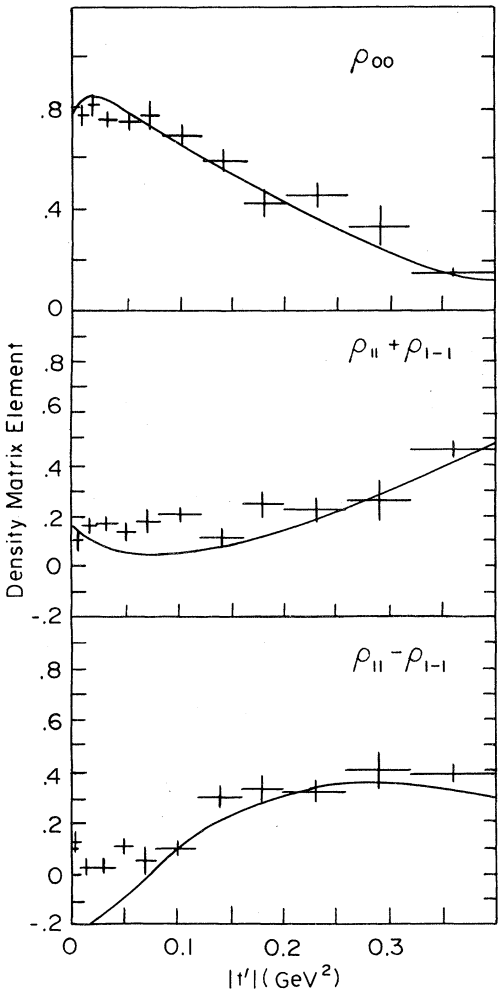

FIG. 12. The ρ^0 density-matrix elements in the helicity frame in the reaction $\pi^- p \to \pi^+ \pi^- n$. (a) ρ_{00}; (b) $\rho_{11}+\rho_{1-1}$; (c) $\rho_{11}-\rho_{1-1}$. The solid curves are the predictions of Ref. 8.

areas in these figures correspond to spectra where $|t'|$ between the remaining particle and the beam (if remaining particle is a meson) or target (if remaining particle is baryon) is less than 0.4 GeV^2. As can be seen there is indication for ρ^- and g^- meson production [Fig. 3(a)], $\Delta^0(1236)$ production [Fig. 3(b)], and $\Delta^+(1236)$ production [Fig. 3(c)], all from reaction (2). These resonances are produced at small momentum transfers. Similarly, the resonances from reaction (3) are produced at low momentum transfers. Similarly, the resonances from reaction (3) are produced at low momentum transfers. From Fig. 4(a) we see that the ρ^0, f^0, and g^0 resonances are copiously produced. From Figs. 4(b) and 4(c) there exists little evidence for any state except possibly for a small enhancement in the Δ^- region [Fig. 4(c)].

The separation of the various resonances in (2) and (3) was carried out using the prism-plot technique.[5] The effective-mass spectra of the resonances considered are shown in Figs. 5 and 6, corresponding to reactions (2) and (3), respectively. The cross sections for the states considered are given in Table III. We have also found evidence for a Δ^- produced by baryon exchange whose cross section is given in Table III, and whose effective mass is indicated by the accumulation of events in the $\Delta(1236)$ region in Fig. 6(c) (shaded events).

From Table III we see that the cross sections for ρ and g production from (2) is more than half those of reaction (3), respectively, which implies that $I=0$ exchange is also involved in reaction (2). Again from isospin arguments assuming $I=1$ exchange we would expect the following ratio:

$$R\left[\frac{\pi^- p \to \pi^- \Delta^+ \to \pi^- p \pi^0}{\pi^- p \to \pi^0 \Delta^0 \to \pi^0 p \pi^-}\right]=2$$

and regardless of the exchange mechanism we would expect

$$R\left[\frac{\pi^- p \to \pi^- \Delta^+ \to \pi^- p \pi^0}{\pi^- p \to \pi^- \Delta^+ \to \pi^- n \pi^+}\right]=2\,.$$

For the latter, we get

$$R=1.61\pm 0.12\,.$$

This deviation may indicate interference of the Δ^+ resonance with diffractive dissociation (see Ref. 5).

The energy dependence of ρ, f, g, and Δ production (Refs. 1, 2, and 6) is displayed in Figs. 7(a)–7(c). Most of the data points, including those from this experiment, follow a $p_{\text{lab}}{}^{-2}$ dependence.

V. STUDY OF RESONANCE PRODUCTION

Differential cross sections in $|t'|$ for the resonances separated by the prism plot are presented in Figs. 8 and 9 from the reactions (2) and (3), respectively. Fits to the form $dN/dt = Ae^{B|t'|}$ for small $|t'|$ yield the slope values B shown in Table IV. As the mass of the resonance increases, B is seen to decrease, illustrating the well-known mass-slope correlation. This result holds separately for both meson and baryon resonances.

The solid curve in Fig. 9(c) is the prediction of a Regge-exchange model for ρ^0 production given by Irving and Michael.[7] In addition to π and A_2 ex-

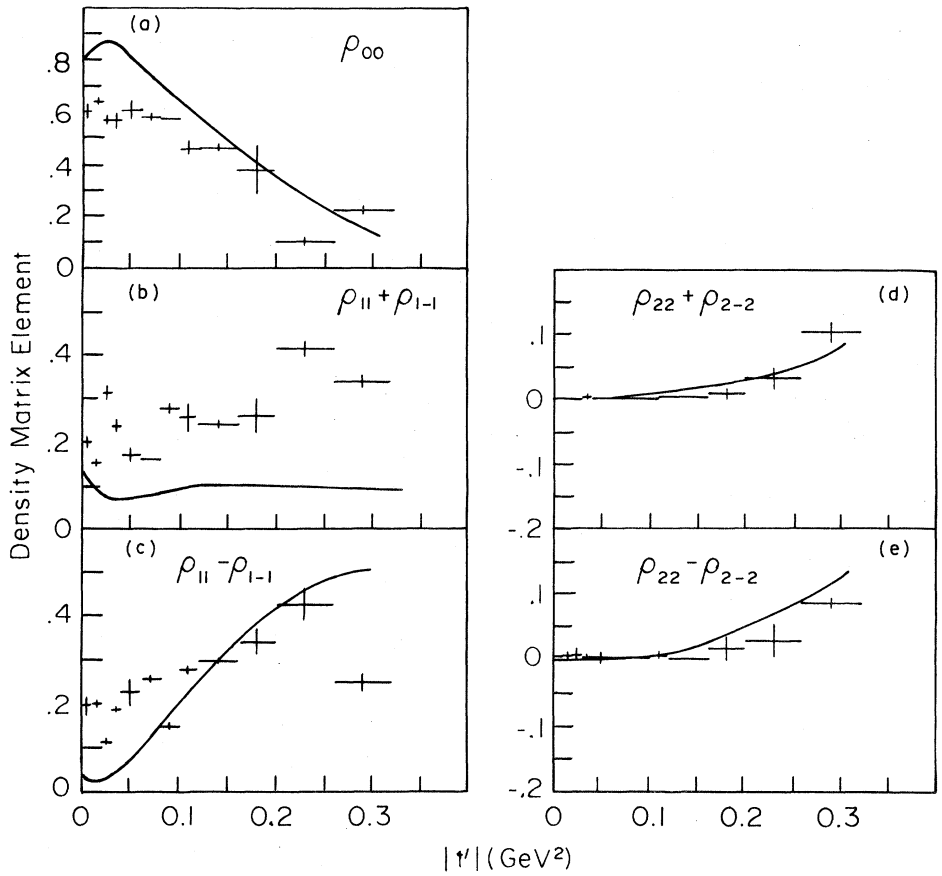

FIG. 13. The f^0 density-matrix elements in the helicity frame in the reaction $\pi^- p \to \pi^+ \pi^- n$. (a) ρ_{00}; (b) $\rho_{11}+\rho_{1-1}$; (c) $\rho_{11}-\rho_{1-1}$; (d) $\rho_{22}+\rho_{2-2}$; (e) $\rho_{22}-\rho_{2-2}$. The solid curves represent the prediction of Ref. 8.

changes, this model includes a cut contribution to account for the nonvanishing differential cross section at $t'=0$ where all Regge contributions vanish. The same exchanges have been used to predict the spectra for f^0 production (curve not shown) and also describes the data well. The similarity of the differential cross section as well as the $P_{\text{lab}}{}^{-2}$ dependence of the total cross section [Fig. 7(b)] for ρ^0 and f^0 production suggests a similarity in their production mechanism. The slope of the g^0 distribution is similar to that of ρ^0 and f^0, suggesting a common production mechanism for the three resonances.

The helicity-frame spin-density-matrix elements ρ_{00}, $\rho_{11}+\rho_{1-1}$, and $\rho_{11}-\rho_{1-1}$ for ρ^- production are plotted as a function of $|t'|$ in Fig. 10. The method used in calculating these density-matrix elements is described in Ref. 8 and is essentially a maximum-likelihood method of simultaneously fitting the mass and angular distributions of the resonance decay products in the helicity frame. Only a P-wave vector meson was assumed in this analysis. As seen in Fig. 10, ρ_{00}, which is a measure of unnatural-parity exchange with no helicity flip, is large at small values of $|t'|$ and falls off rapidly with increasing $|t'|$. As for the natural-parity-exchange contribution measured by $\rho_{00}+\rho_{1-1}$, it is consistent with zero at $|t'| \sim 0$ and rises abruptly, becoming the largest exchange contribution at $|t'| = 0.15$ GeV^2. The contribution of the unnatural-parity-exchange helicity flip, which is measured by $\rho_{11}-\rho_{1-1}$, is very small at small $|t'|$ and rises linearly becoming equal to $\rho_{11}+\rho_{1-1}$ at about $|t'| = 0.4$ GeV^2. These observations suggest the dominance of π exchange without helicity flip for $|t'| \lesssim 0.1$ (as expected, since helicity flip is not possible at small $|t'|$), whereas ω exchange also begins to play an important role at $|t'| \sim 0.15$ GeV^2. In the higher-$|t'|$ region, exchange of higher-mass mesons such as the A_1 may also be important, in addition to π exchange with helicity flip.

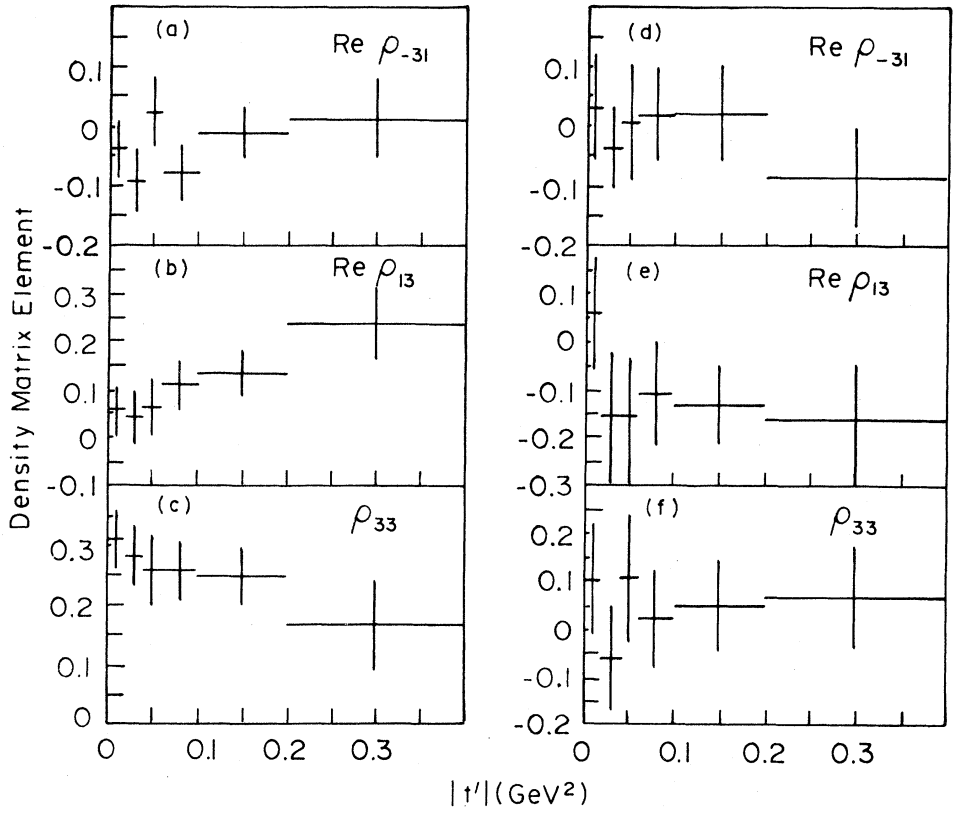

FIG. 14. The Δ^+ and Δ^- density-matrix elements in the Gottfried-Jackson frame in the reaction $\pi^- p \to \pi^+ \pi^- n$. (a) Re$\rho_{-31}$; (b) Re$\rho_{13}$; (c) ρ_{33}; (d) Reρ_{-31}; (e) Reρ_{13}; (f) ρ_{33}. (a)—(c) refer to Δ^+ and (d)—(f) refer to Δ^-.

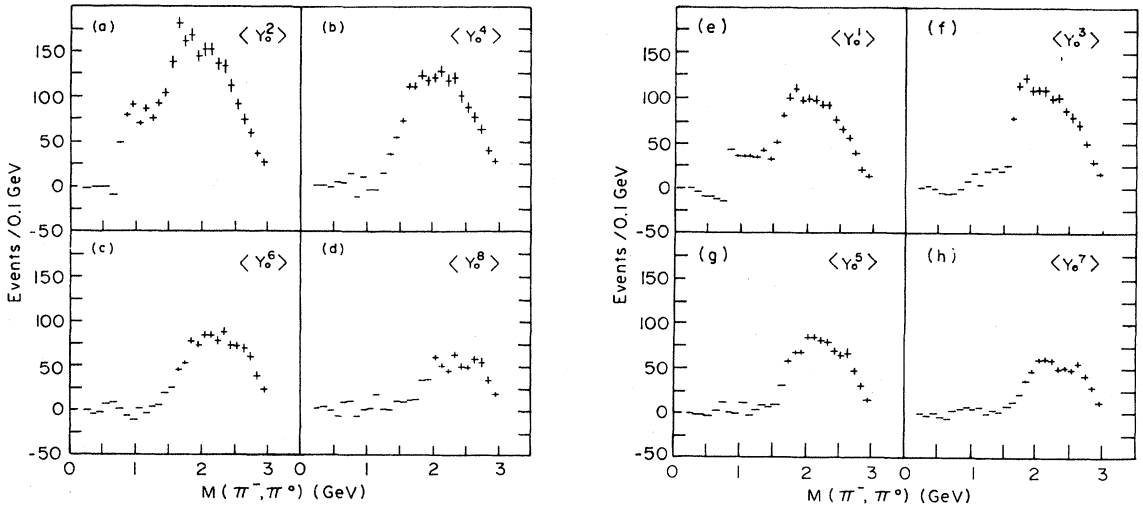

FIG. 15. The Y_0^L moment distributions as a function of $M(\pi^- \pi^0_=)$ in the reaction $\pi^- p \to \pi^- \pi^0 p$. (a) $N\langle Y_0^2 \rangle$; (b) $N\langle Y_0^4 \rangle$; (c) $N\langle Y_0^6 \rangle$; (d) $N\langle Y_0^8 \rangle$; (e) $N\langle Y_0^1 \rangle$; (f) $N\langle Y_0^3 \rangle$; (g) $N\langle Y_0^5 \rangle$; (h) $N\langle Y_0^7 \rangle$ where N is the number of events in the distribution.

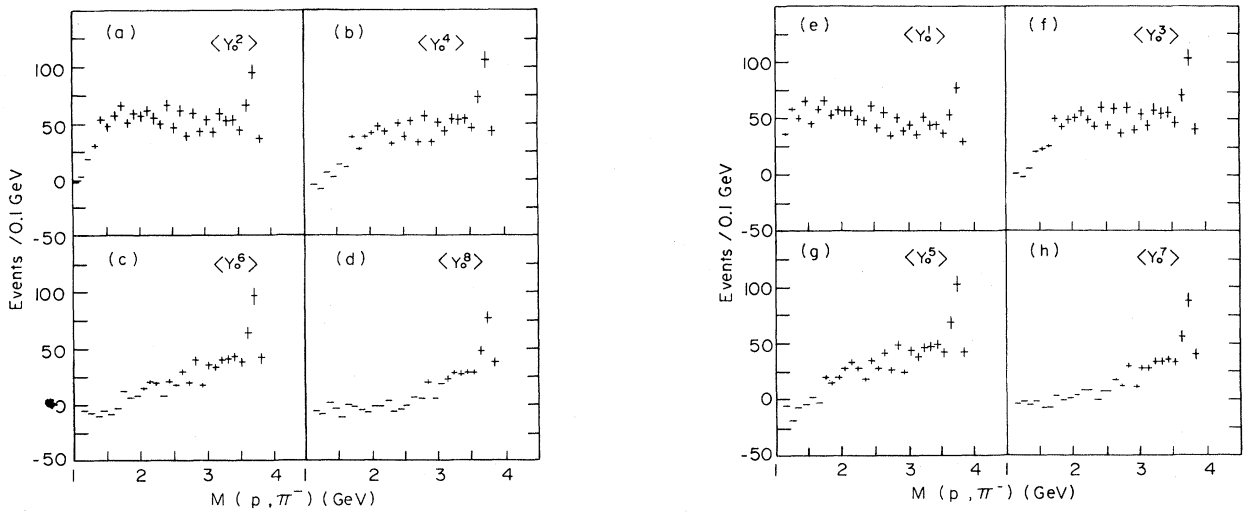

FIG. 16. As in Fig. 15 for $M(\pi^- p)$.

The density-matrix elements for the Δ^+ and Δ^0 resonances from reaction (2) are plotted in Fig. 11 in the Gottfried-Jackson frame. For the lowest $|t'|$, ρ_{33} is seen to dominate with values near 0.3. We recall that for pion exchange, which is forbidden by G parity in this reaction, $\rho_{33}=0$. It is seen that $\mathrm{Re}\rho_{13}$ has a value consistent with zero for all $|t'|$ and that $\mathrm{Re}\rho_{-31}$ rises with $|t'|$ from zero to about 0.1 for Δ^+ but is consistent (for most $|t'|$) with zero for Δ^0. The Sakurai-Stodolsky model for ρ exchange in analogy with photon exchange predicts $\rho_{33}=0.375$, $\mathrm{Re}\rho_{3-1}=0.216$, and $\mathrm{Re}\rho_{13}=0$, so that the model is not very successful in describing the data.

Spin-density-matrix elements ρ_{00}, $\rho_{11}+\rho_{1-1}$, and $\rho_{11}-\rho_{1-1}$ for ρ^0 production (helicity frame) are shown in Fig. 12 as a function of $|t'|$. An S-wave background under the P-wave vector-meson signal was included when calculating the density-matrix elements. This method, based on the assumption that mass and angular dependences for the amplitudes can be factorized, is believed to properly treat interference effects between resonance and background waves.[8]

The prediction of a Regge-exchange model[7] as a function of $|t'|$ is shown as a solid curve in Fig. 12 and, as with the prediction for the ρ^0 differential cross section, the model describes the data well.

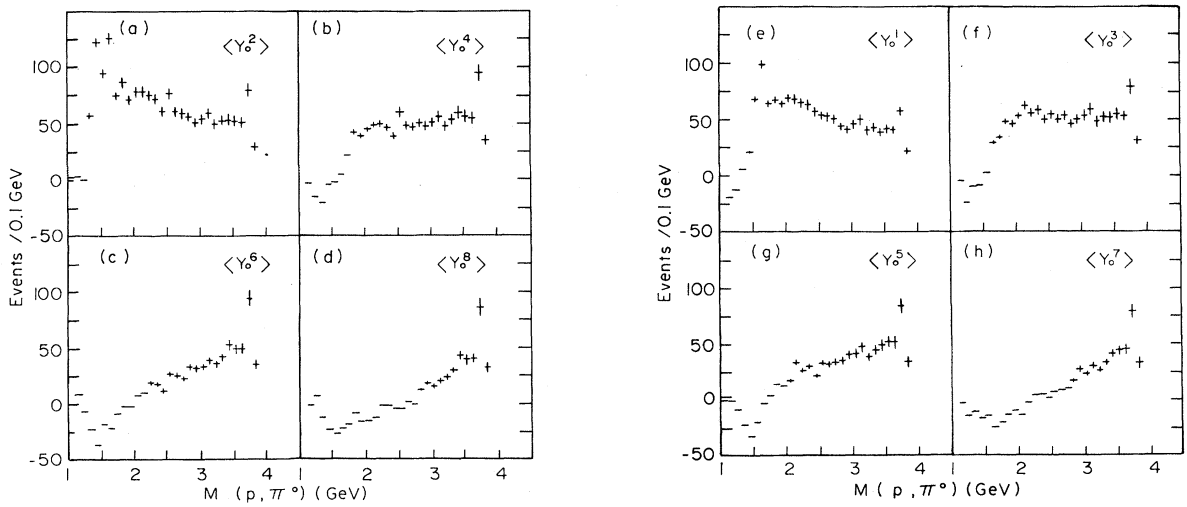

FIG. 17. As in Fig. 15 for $M(\pi^0 p)$

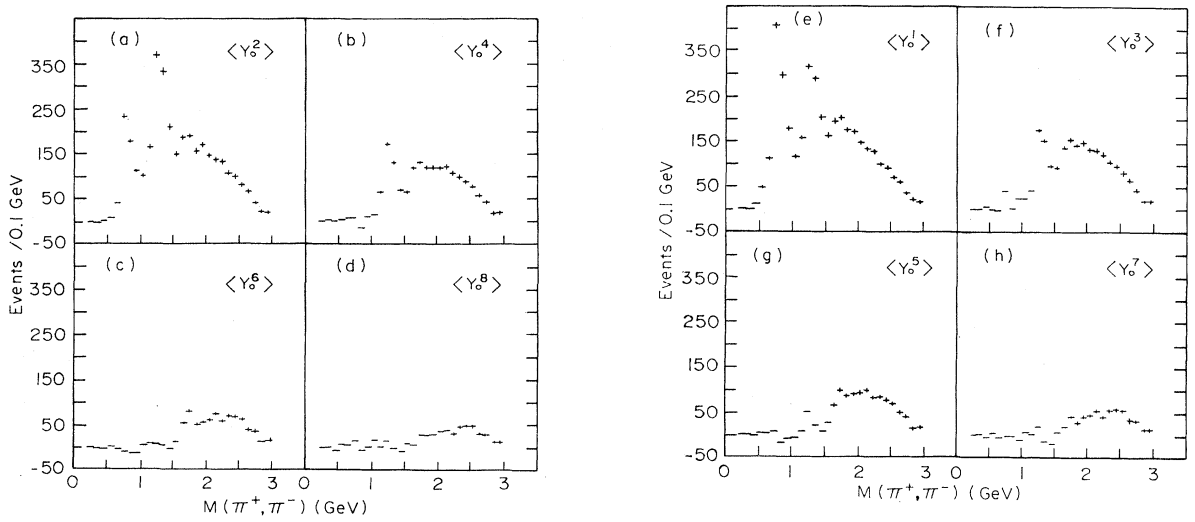

FIG. 18. As in Fig. 15 for $M(\pi^+\pi^-)$ in the reaction $\pi^- p \to \pi^+\pi^- n$.

It is seen that ρ_{00} is large for small $|t'|$ values, indicating the importance of π exchange without helicity flip. The combination ρ_{11}-ρ_{1-1} is small at low $|t'|$ and increases for higher $|t'|$ values, suggesting a helicity-flip contribution. The natural-parity-exchange (A_2) contribution is small and nearly constant up to $|t'| = 0.3$ GeV^2.

The f^0 density-matrix elements have been evaluated including only *S-D* interference (for details see Ref. 8), since the presence of *S* and *P* background waves under the *D* wave of the f^0 raises the number of independence matrix elements to 27. According to Ref. 6, the *P*-wave contributions are consistent with zero at 12 and 15 GeV/*c* incident π^- momenta, and, therefore, it was not included here.

The values of the density-matrix elements shown in Fig. 13 are evaluated in the helicity frame and represent an average of the results obtained when assuming maximal and minimal *S-D* interference. The error bars shown include both statistical errors plus the range allowed by maximal and minimal *S-D* interference. The solid curves in Fig. 13 represent the Regge-model[7] predictions.

The similarity between ρ_{00}, $\rho_{11}+\rho_{1-1}$ and $\rho_{11}-\rho_{1-1}$ for ρ^0 and f^0 production as a function of $|t'|$ suggest that their production mechanisms are similar. The elements $\rho_{22}-\rho_{2-2}$ are consistent with zero up to $|t'| = 0.3$ GeV^2, implying the absence of a helicity flip of 2.

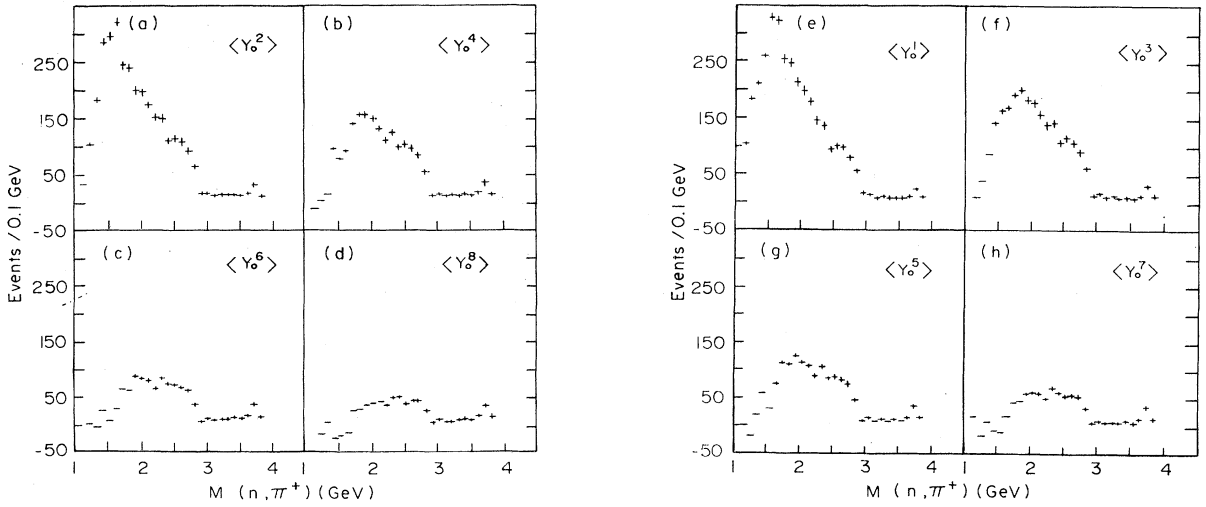

FIG. 19. As in Fig. 18 for $M(n\pi^+)$.

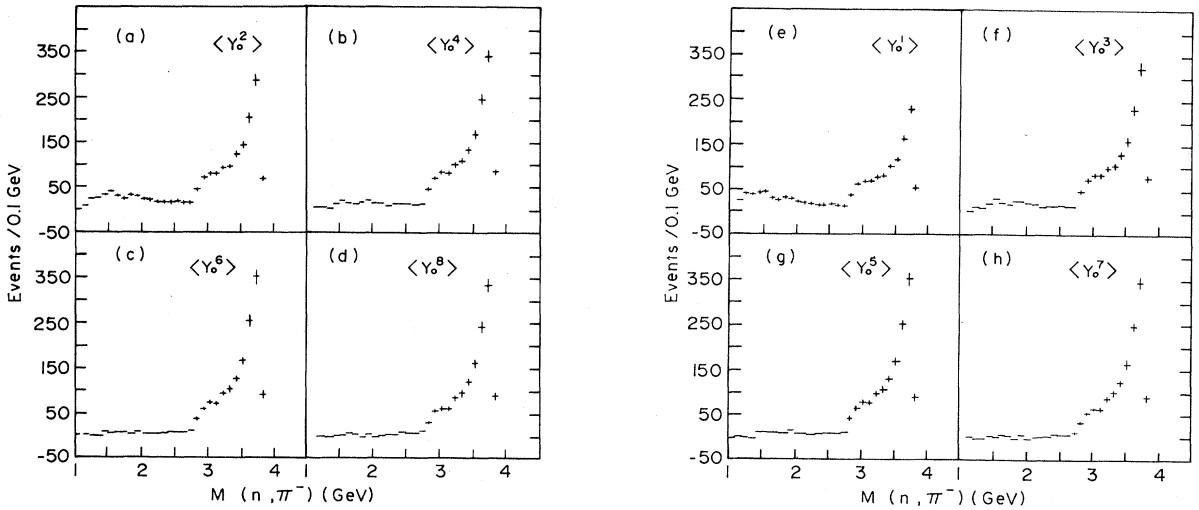

FIG. 20. As in Fig. 18 for $M(n\pi^-)$.

The spin-density-matrix elements were not determined, since an analysis requires S, P, D, and F waves with their interferences, thus involving a large number of parameters.

The Gottfried-Jackson-frame density-matrix elements of the Δ's have been evaluated for reaction (3) and are plotted in Fig. 14. For Δ^+ production the ρ_{33} element is similar in its $|t'|$ dependence as in reaction (2). It is seen that $\mathrm{Re}\rho_{13}$ rises from zero with $|t'|$ in disagreement with the Sakurai-Stodolsky prediction. The production of Δ^- involves an exotic exchange and, therefore, the spin-density-matrix elements are not expected to behave as those of Δ^+. Indeed, it is seen in Fig. 14(f) that ρ_{33} is consistent with zero for all $|t'|$ instead of falling with $|t'|$ from a value of about 0.3

The unnormalized Legendre-polynomial moment distributions as a function of the effective mass of a two-body state gives information about the spin content of the two-body system. These spectra are illustrated in Figs. 15–20 for $|t'| \leq 0.4$ GeV^2 for Y_0^L moments where $L = 1-8$. We note that nonvanishing values for odd L imply interference between states of opposite parity, whereas nonvanishing values for even L imply either pure spin states or interference between states of the same parity.

In Fig. 15 the moments for the $\pi^-\pi^0$ invariant mass is plotted. No clear evidence for a peak at 1680 GeV (g) is evident although all moments for $L = 1-6$ are rising in this region and those for $L = 7,8$ are consistent with zero. The detailed nature of the interference of the spin-3 g^- meson with the background may cause the absence of a peak.

In the case of the baryon resonances, the signals do not stand out clearly above the background (see Fig. 4). The moments are presented for $p\pi^-$ and for $p\pi^0$ in Figs. 16 and 17, respectively. The even moments $L = 6,8$ in Fig. 16 are consistent with zero for masses below ~ 1800 MeV, suggesting that states of spin $> \frac{5}{2}$ do not contribute in the resonance region. This is not the case for $p\pi^0$ states, however (Fig. 17). The $L = 1$ moments for both reactions show structure in the Δ region which implies an interference with the Δ of spin-parity $\frac{1}{2}^-$ or $\frac{5}{2}^-$ states. The presence of such states, which earlier analysis[9] has indicated to be diffractively produced, would represent a violation of the Gribov-Morrison rule.[10] This empirical rule states that diffractively produced systems obey the relation

$$\Delta P = (-1)^{\Delta J},$$

where ΔP and ΔJ are the changes in parity and angular momentum between the projectile and diffractive systems. Although the rule holds with at most a violation of 5–10% for most mesonic diffractive systems, it seems to be strongly violated in the case of nucleon-induced diffractive dissociation.[11]

The $\pi^+\pi^-$ moments from reaction (3) are plotted in Fig. 18. The $L = 2$ moment has a clear peak in the ρ^0 region, the $L = 4$ moment has a clear peak in the f^0 region, and a peak is discernible for the

$L=6$ moment in the g^0 region with no structure in these regions for $L=8$. The moments also suggest interference in these resonance regions. The peaks in the $L=1$ moment in the ρ and f resonance regions suggest interference of these resonances with S and P waves, respectively. The peak in the $L=2$ moment in the f region may indicate S-wave interference with the f, whereas the peak in this region for $L=3$ is suggestive of a P-wave background to the f. The enhancement in the $L=3$ moment in the g suggests S-wave interference. Also, the enhancements in the g region for the $L=4$ and $L=5$ moments suggest P- and D-wave interferences, respectively, with the g.

The moments for $n\pi^+$ are presented in Fig. 19. It is seen that below ~ 1800 MeV states up to spin$=\frac{7}{2}$ contribute [Fig. 19(c)]. The odd moments show significant interference effects including the violation of the Gribov-Morrison rule, as in the $p\pi^0$ case. Clearly, many states contribute and the interferences are significant.

The $n\pi^-$ moments (Fig. 20) show little structure throughout the resonance region.

VI. CONCLUSIONS

Results from a high-statistics bubble-chamber experiment on $\pi^- p$ elastic and two-prong one-constraint inelastic scattering at 8 GeV/c are presented. The channel cross sections have been obtained by the prism-plot separation. Significant ρ^-, g^-, and ρ^0, f^0, g^0, Δ^+, Δ^0, Δ^-, $N^*(1470)$ and $N^*(1688)$ production are seen. Spin-density-matrix-element analysis for the ρ^0, f^0, and ρ^- mesons lends support to the idea that the ρ^0 and f^0 have similar production mechanisms. The ρ^- analysis indicates that π exchange without helicity flip is dominant at $|t'| \leq 0.1$ GeV^2 while for $|t'| > 0.15$ GeV^2 exchange of other particles becomes important. A Regge-exchange model[8] gives a good description of the ρ^0 and f^0 production and decay. The nucleon-pion invariant-mass spectrum is complicated by significant interference between various states. This is most clearly seen in the moments for the $n\pi^+$ effective mass. As seen previously the Δ^+ production has as a background a diffractive component violating the Gribov-Morrison rule.

ACKNOWLEDGMENTS

We wish to thank the SLAC bubble-chamber operating crew for its professional operation of the bubble chamber and the quality of the film. We also wish to thank the data-reduction teams at Tohoku University, Massachusetts Insitute of Technology, Oak Ridge National Laboratory, and the University of Tennessee, whose dedicated efforts made this experiment possible. This work was supported in part by the United States Department of Energy, the National Science Foundation, and the Japan Society for the Promotion of Science.

---

[a]Now at Heidelberg University, West Germany.
[b]Now at Tufts University, Medford, Massachusetts 02155.
[c]Now at Mitsui-Joho KK, Tokyo, Japan.
[d]Now at DESY, Hamburg, West Germany.
[e]Permanent address: Tel-Aviv University, Ramat-Aviv, Israel.
[f]Now at SLAC, Stanford, California 94305.
[g]Permanent address: Istituto di Fisica Nucleare, Pavia, Italy.
[h]Now at Weizmann Institute, Rehovot, Israel.
[i]Now at CERN, Geneva 23, Switzerland.
[j]Permanent address: Nara Women's University, Nara, Japan.
[k]Now at Rockefeller University, New York, New York 10021.
[l]Now at Automatix, Burlington, Massachusetts 01803.
[m]Now at Bell Laboratories, Naperville, Illinois 60540.
[n]Permanent address: Inst. of High Energy Physics, Beijing, China.

[1]E. Bracci *et al.* CERN/HERA Report No. 72-1 (unpublished); Particle Data Group, Report No. LBL-90 (unpublished).
[2]E. W. Anderson *et al.*, Phys. Rev. Lett. 25, 699 (1970).
[3]A. Eide *et al.*, Nucl. Phys. B 60, 173 (1973); C. T. Coffin *et al.*, Phys. Rev. 159, 1169 (1967); I. Amfats *et al.*, Phys. Rev. D 9, 1179 (1974); D. Harting *et al.*, Nuovo Cimento 38, 60 (1965).
[4]D. P. Owen *et al.*, Phys. Rev. 181, 1794 (1969); N. Sharfman *et al.*, Phys. Rev. Lett. 40, 681 (1978); E. W. Anderson *et al.*, *ibid.* 20, 1529 (1968).
[5]G. Berlad *et al.*, Nucl. Phys. B78, 29 (1974).
[6]G. Alexander *et al.*, Nucl. Phys. B131, 365 (1977).
[7]A. C. Irving and C. Michael, Nucl. Phys. B82, 282

(1974).
[8]M. Aguilar-Benitez *et al.*, Phys. Rev. D 6, 11 (1972).
[9]J. V. Beaupré, Nucl. Phys. B66, 93 (1973).
[10]V. N. Gribov, Yad. Fiz. 5, 197 (1966); [Sov. J. Nucl. Phys. 5, 138 (1966)]; D. R. O. Morrison, Phys. Rev. 165, 1699 (1968).
[11]D. Sotiriou, Nucl. Phys. B107, 457 (1976); W. Ochs *et al.*, *ibid.* B86, 253 (1975).